Summer 2012

A planning tool to predict the welding angle in laser metal deposition

Sriram Prabhu

Department:

A PLANNING TOOL TO PREDICT THE WELDING ANGLE IN LASER METAL DEPOSITION

By

SRIRAM PRABHU

A THESIS

Presented to the Faculty of the Graduate School of the

MISSOURI UNIVERSITY OF SCIENCE AND TECHNOLOGY

In Partial Fulfillment of the Requirements for the Degree

MASTER OF SCIENCE IN MANUFACTURING ENGINEERING

2012

Approved by

Dr. Frank Liou, Advisor
Dr. Elizabeth Cudney
Dr. Susan Murray

PUBLICATION THESIS OPTION

This thesis is composed of one paper which was reformatted in the style used by the university.

The paper presented in pages 4-46 titled “A PLANNING TOOL TO PREDICT THE WELDING ANGLE IN LASER METAL DEPOSITION” is intended for submission to INTERNATIONAL JOURNAL OF PRECISION ENGINEERING AND MANUFACTURING.

ABSTRACT

Research in Laser Metal Deposition (LMD) has been done rigorously in the past. However, the main challenge that still exists is the production of complex part geometries having overhang features. Production of such features requires individual tracks with a high aspect ratio and wider bead angle. The use of destructible/ non-destructible support structures involves costly post production operations which increase production cost. Tilting or moving the deposition surface can be useful to create overhangs but are applicable only to special cases. Since such techniques have to be used by the manufacturing community, the techniques need to be simple in calculation and easy to understand.

The paper presented in this thesis presents a novel technique of depositing a track having a wide welding angle. This novel method solves the above mentioned challenge by depositing tracks having the capability to build overhang features. The new approach that has been implemented in this paper involves using the energy balance to estimate the amount of superheat present in the melt pool and correlating it with the weld bead angle. Attention has been paid to make the model computationally less cumbersome.

Furthermore, the technique has been applied to a produce a couple of tracks with predetermined welding angles successfully.

ACKNOWLEDGMENT

This research work is a result of some phenomenal help and support extended to me by many individuals at Missouri S&T. I would like to express my sincere gratitude towards my advisor Dr. Frank Liou for his continued guidance, encouragement and co-operation throughout my research work. It has been a great pleasure working with the entire team at the LAMP lab over the past two years and without their help this work would not have been possible. The research assistantship extended to me by Dr. Liou through the Manufacturing Engineering Program is also greatly acknowledged.

I would also like to thank my committee members Dr. Elizabeth Cudney and Dr. Susan Murray for the time and advice they granted to me during the research. I would like to express my sincere thanks to Dr. Jianzhong Ruan, Todd Sparks, and Jomy Francis for being available whenever I needed their help. A special thanks to my friend Sushrut Bapat for helping me intensively during the modeling stages. I sincerely would also like to thank Aashiesh Avachaat, Avinash Raju, Tarak Amine, and Abhishek Kumar for helping me during my experiments and providing me with valuable suggestions which have been very critical in completing my research work. I can never forget my roommates at Rolla; Sudhanwa, Zafar, and Sandeep who became my pillars of strength during my stay for the past two years.

Finally, I would like to express my gratitude towards my parents, Mr. Sirish Prabhu, Prof. Tejovati Prabhu, and my sister Vandita Prabhu-Mahale for their unconditional love and support and God Almighty for guiding me throughout the various stages of my life.

TABLE OF CONTENTS

Page

PUBLICATION THESIS OPTION iii

ABSTRACT iv

ACKNOWLEDGMENT v

LIST OF ILLUSTRATIONS viii

LIST OF TABLES x

SECTION

1. INTRODUCTION 1

1.1. OBJECTIVE 1

1.2. BACKGROUND AND PROPOSED TECHNIQUES 1

1.3. CONTRIBUTIONS 2

PAPER

A PLANNING TOOL TO PREDICT THE WELDING ANGLE IN LASER METAL DEPOSTION 4

Abstract 4

1. INTRODUCTION 5

2. LITERATURE REVIEW 8

2.1. TEMPERATURE MEASUREMENT 10

3. NOMENCLATURE 13

4. MODEL FORMULATION 14

4.1. BASIC ASSUMPTIONS 14

4.2. ASSUMPTION OF VALUES 14

4.3. EXPERIMENTAL ASSUMPTIONS 15
4.4. MASS BALANCE 16
4.5. ENERGY BALANCE 19
4.5.1. Formation of Melt Pool 21
4.5.2. Energy Loss from the System 22
5. MODEL VERIFICATION AND DISCUSSION 26
5.1. EXPERIMENTAL PROCEDURE 26
5.2. MELT POOL TEMPERATURE PREDICTION 29
5.3. HEIGHT PREDICTION 31
5.4. THE WELD BEAD ANGLE, ASPECT RATIO AND THE SUPERHEAT .. 34
5.5. VARIATION IN THE WIDTH OF THE WELD BEAD 37
5.6. ENERGY DISTRIBUTION 39
6. MODEL APPLICATION 42
7. CONCLUSION 46
8. ACKNOWLEDGEMENT 47
9. REFERENCES 48
VITA 51

LIST OF ILLUSTRATIONS

Figure Page

1. A 316L stainless steel part deposition from initial to final stage.....5

2. A schematic diagram of the LMD process. 6

3. Cross-section of three different types of track profiles for single track deposition beads.....8

4. A photograph showing the rapid solidification of the melt pool during metal deposition process.....11

5. Representation of the mass both entering in and sustained by the system during deposition.....16

6. Photograph of the powder flow process shot during the experiment.....17

7. Energy balance of the deposition process.....19

8. The transition of the melt pool from circle to ellipse during the deposition process.....21

9. Diagrammatic representation of the experimental set up. 26

10. Measurement of bead geometry.....29

11. Comparison of the modeled and the experimental results of the temperature in the melt pool. 30

12. Macrographs of the bead geometries deposited during the experiments.....32

13. Comparison of the predicted and measured heights of the deposited tracks without the error function 32

14. Comparison of the modeled and the measured height after the use of error function. 33

15. Comparison of the amount of superheat with the weld bead angle and the aspect ratio of the beads.....35

16. Effect of the positive and negative value of $\boldsymbol{\partial\sigma/\partial T}$ in the weld bead. 36

17. Comparison of the width of the weld bead with the energy utilized during the process.....38

18. Variation of the bead with interaction time for different laser power and mass flow rates.....39

19. Average distribution of modeled energy lost from the system. 40

20. Variation of the weld bead angle with the amount of superheat.....42

21. Schematic diagram of the flowchart of the proposed model. 44

22. Macrographs of the deposited track with a pre-determined bead angle at 100X magnification. 45

LIST OF TABLES

Table Page

1. Thermo-physical properties of the materials used during the experiment. 27

2. Process parameters used for the experiment. 29

3. Results of ANOVA performed between the experimentally measured and modeled melt pool temperatures. 31

4. Results of ANOVA performed between the experimentally measured and modeled weld bead height. 34

5. Properties for the track deposited using the model.. 45

1. INTRODUCTION

1.1. OBJECTIVE

The use of Laser Metal Deposition (LMD) for the production of part geometries by the manufacturing community has one major challenge, which is the incapability of the process to produce part geometries with overhangs. Typically, overhangs are features which require support structures for it to be built. The use of support structures increases the post processing operations and thus, increases the manufacturing cost. The basic idea in this research is to keep the model as simple as possible so as to present a technique that is viable to implement for real time processing. Thus, this research aims at solving the major challenge of producing tracks that has the capability of building overhanging structures.

1.2. BACKGROUND AND PROPOSED TECHNIQUES

LMD is an additive manufacturing process. The main applications of this process are in part repairs and generation of part geometries and prototypes. The starting material for LMD is in the form of powder of which the part geometry/prototype is to be produced. LMD uses layer-by-layer deposition technique. In this technique, the part geometry is produced by depositing each layer on top of a previously deposited layer based on the path planning strategy. Once powder has been melted by laser according to the part geometry, it is said to be deposited. The final part geometry needs further finish machining operations to have the customer specified surface finish.

Often the part geometries to be produced are made of overhanging features. A common practice has been to deposit the part geometry ignoring the overhang features. Once the geometry is produced the features are then machined out in the post production process along with the finishing operation. However by doing so, the entire concept of additive manufacturing may be lost. Since, this would involve the same amount of material wastage and same amount of machining as it would be required by conventional manufacturing techniques. A universal solution to the problem of depositing overhanging features lies in depositing tracks with a high welding angle and a suitable aspect ratio.

Superheat is the additional amount of heat present in the material above its liquidus temperature. The method of using the superheat which is present in the melt pool; to manipulate the bead geometry has not been reported. This paper aims at using the above mentioned technique to produce tracks with previously decided welding angle.

This research incorporates the various established techniques to predict the melt pool temperature which gives an estimate of the amount of superheat and adds to it the relation between superheat and the weld bead angle. This new approach has the main inclination towards simplicity in calculation which makes it a viable process design tool for the manufacturing engineer.

1.3. CONTRIBUTIONS

Listed below are the contributions of the paper.

- A novel technique to deposit single track with a specific bead angle has been proposed. The model can modestly estimate the amount of superheat present in the melt pool.

- The approach presented in this paper is computationally less cumbersome and thus, aims in being a handy planning tool for the manufacturing engineer to select the process parameters for deposition.
- A relationship between the weld bead angle and the superheat present in the melt pool has been developed and validated with examples.

PAPER

A PLANNING TOOL TO PREDICT THE WELDING ANGLE IN LASER METAL DEPOSITION

Sriram Prabhu[1], Jianzhong Ruan[2] and Frank Liou[3]

[1]Missouri University of Science and Technology, ssptpc@mst.edu
[2]Missouri University of Science and Technology, jzruan@gmail.com
[3]Missouri University of Science and Technology, liou@mst.edu

Abstract

Laser Metal Deposition (LMD) is one of the additive manufacturing processes used to produce fully functional metal parts. A deep understanding of the inter-relationship between process parameters is required to produce a high quality part. The geometry of the deposited track is largely controlled by the temperature of the melt pool. Thus the geometry plays an important role in determining both the quality and the morphology of the part. This paper presents an analytical model that predicts the mean melt pool temperature. This analytical model can also be used for a process design of a deposition tool path with a specified weld bead angle. This model was established to illustrate the effect of the superheat present in the melt pool on the weld bead geometry. The influence of the melt pool temperature on the weld bead angle, height, and width was then studied. The model was verified by helping successfully applied to produce a weld bead with a specified bead angle.

Keywords: Weld Bead Angle, Superheat, Energy Balance, Laser Metal Deposition.

1. INTRODUCTION

Rapid manufacturing technologies have been developed, though the production of functional parts needs further development. The Laser Metal Deposition (LMD) process is one of the rapid manufacturing technologies capable of producing fully functional metal components directly from a CAD model. LMD is an extension of the cladding process which has been successfully applied to cladding, coating, and repair.

Rapid prototyping, the manufacturing of functionally graded materials and production of fully functional components are being carried out but with some difficulties in certain part geometries. Traditional manufacturing involves material removal to produce the desired part geometry. Material removed therein is both wasted and accounted for during the billing process. On the contrary, LMD builds the part geometry layer by layer thus utilizing the material efficiently. Figure 1 gives a glimpse of part production by LMD process.

(a) (b) (c)

Fig. 1 A 316L stainless steel part deposition from initial to final stage. Here, Figure (a) shows the layer-by-layer part deposition. Figure (b) shows the part just after deposition and Figure (c) shows the final part after finishing operation.

The deposition process is illustrated in Figure 2. The laser beam, which is coaxial with the nozzle, is focused to form a melt pool on the surface of the substrate. In the current experimental set-up, the nozzle used to emit the laser is also used to supply the powder to the melt pool. Deposition systems, however, also consist of set-up where the powder sprayed in the melt pool is not coaxial with the nozzle. A carrier gas transports the powder particles through the nozzle in the melt pool. The powder, while travelling through the nozzle, absorbs some heat from the laser. Thus, some of the powder is melted while travelling from the nozzle to the melt pool. As the nozzle moves ahead, both the laser beam and the substrate move relatively opposite to one another, the powder injected in the melt pool becomes quickly solidified generating a raised (deposited) track.

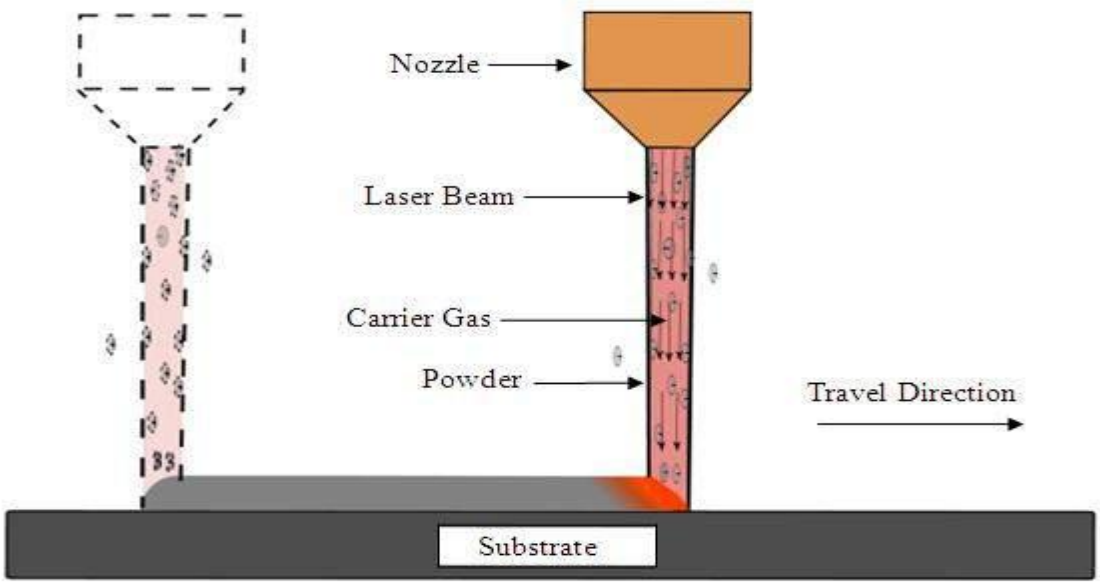

Fig. 2 A schematic diagram of the LMD process.

As this process continues, a small, deposited track consisting of melted material is generated. The melt pool follows the laser beam which moves according to either the desired part geometry or the build direction. The LMD process involves a complex interrelationship between the process parameters (laser power, powder flow rate, and table speed) and the physical quantities (e.g., temperature of the melt pool, material in concern, weld bead angle, and aspect ratio) involved. Thus, understanding a quantitative influence of process parameters on the different physical quantities of interest is required.

2. LITERATURE REVIEW

Many analytical and numerical models have explicitly highlighted the important phenomena such as heat conduction, thermo-capillary flow, laser power attenuation due to powder flow, and laser power absorption on process characteristics. Weeresinghe and Steen [1] developed a simple linear relationship between process parameters, such as both table speed and track width for single tracks and proposed three basic clad section profiles as shown in Figure 3 .

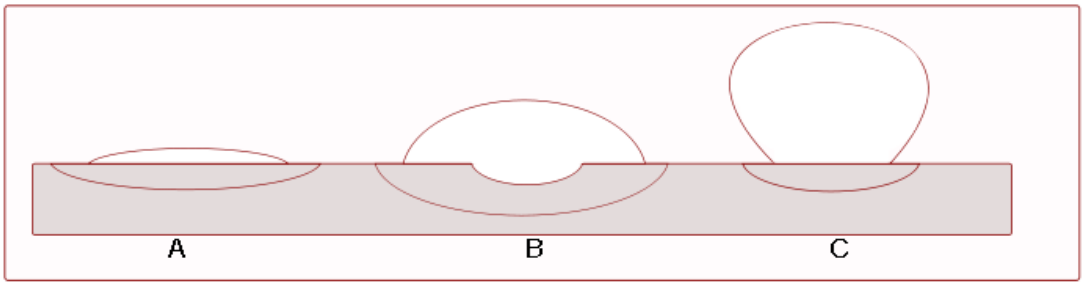

Fig. 3 Cross-section of three different types of track profiles for single track deposition beads.

Colaco et al. [2] developed one of the early models for single track geometry. This model, however was based only on powder flow. Kar and Mazumdar [3] studied both the composition of alloys and the cooling rate during the laser cladding process by developing a one-dimensional heat conduction equation. Jouvard et al. [4] proposed power thresholds for successful deposition of single-track beads by studying the interaction of the laser beam with both the powder and the substrate. Gedda et al. [5] used both experimental and theoretical methods to estimate the energy distribution during the

complete Direct Metal Deposition (DMD) process. They compared both Nd:YAG and CO_2 laser sources, concluding that the latter was half as efficient as the former in terms of power source.

Pinkerton and Li [6] created an energy balance to demonstrate the effect of the coupling efficiency on the DMD process. They considered the effect of the absorption capacity of the substrate for each of the three laser sources: e.g., CO_2, Nd:YAG, and HPDL (High Power Diode Laser) sources. Pinkerton and Li [6] concentrated on the comparison of energy loss by conduction, convection, radiation and evaporation when using the above mentioned three laser sources. Their model, however, did not account for the effect of table speed.

Toyserkani et al. [7] studied the effect of powder feed rate, process speed, and laser power on clad characteristics by developing a three-dimensional, finite element model. Liu and Lin [8] investigated the interaction between the laser and powder. They studied the powder heating process by considering each particle as a single spherical particle. The focus of previous research had concentrated heavily on type track profiles ‘A’ and ‘B’, illustrated in Figure 3. These studies approximated the cross-section of the melt pool (in the horizontal X-Y plane) as an ellipse. Thus, the previous research was narrowed to focus on both type track profiles ‘A’ and B’.

Porosity, poor surface finish, and quality are the primary reasons type track profile ‘C’ was excluded. The analysis, however, of multiple-layer, single track width geometries led to the conclusion that the constituent track does contain ‘C’ type profiles. Moreover, the inclusion of type track profile ‘C’ does not produce any kind of non-

conformity as they become re-melted during the deposition of the next layer [7]. Thus in this paper a fairly novel approach is established to investigate the wetting angle of the deposited track with respect to the temperature of the melt pool.

Multiple factors have been shown to be responsible for weld bead morphology. Much research has been done to investigate these factors. Most of this research concentrated on ‘A’ and ‘B’ type profiles. This paper presents both an analytical model and an experimental set-up to investigate the effect of process parameters: laser power, powder mass flow, scanning speed, and the melt pool thermal behavior. Analytical models were developed using mass, momentum and energy balances across the melt pool, both with and without the effects of phase change. This paper presents a simple analytical model that describes the weld bead geometry of a single-track deposition based on both energy and mass transfer during the metal deposition process.

2.1. TEMPERATURE MEASUREMENT

Generally, two techniques which have been widely used to report the temperature measurement during metal deposition are:

- Contact measurements such as thermocouples which provide efficient ways of measuring temperature. Thermocouples are inserted into a substrate on which the deposition is to be made [9, 10]. They are used extensively when the temperature history of either the substrate or the temperature near the melt pool is to be recorded. Depositing on the thermocouples to measure the temperature of the melt

pool has resulted in melting the thermocouple. Making it incapable of measuring temperature.

- Non-contact measurement such as radiation pyrometer which consists of an optical system and detector. Any object at a temperature higher than absolute zero emits electromagnetic radiation. The optical system focuses the electromagnetic radiation emitted by an object onto the detector. The output of the detector is proportional to the amount of energy radiated by the object. This output can be used to infer the object's temperature. The emittivity, or emittance, of the object is an important variable in converting the detector output into an accurate temperature signal.

LMD is a rapid solidification process that occurs under non-equilibrium conditions. Solidification is completed in a fraction of a second. Figure 4 is a photo of a melt pool during the deposition process.

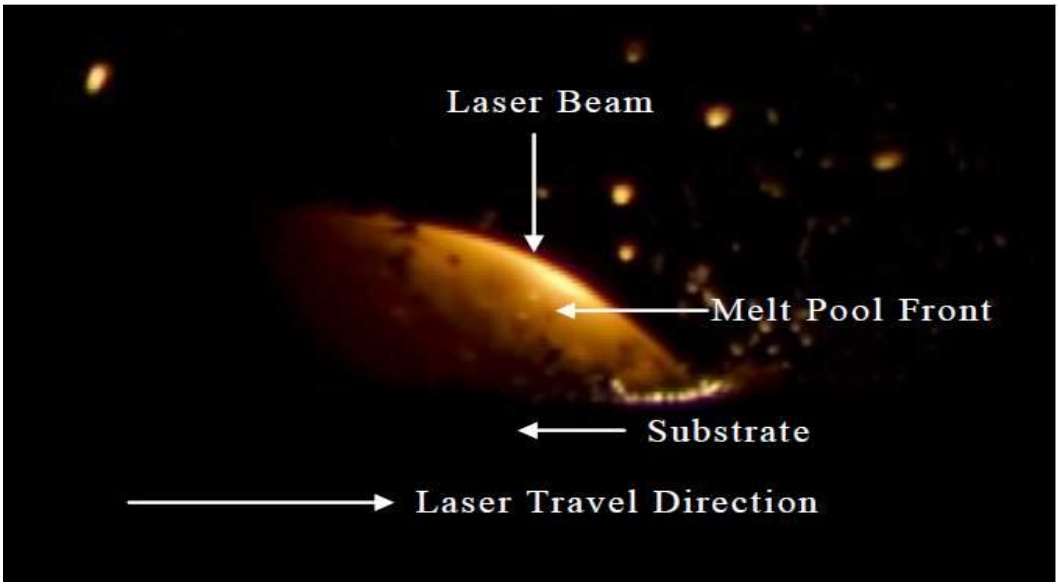

Fig. 4 A photograph showing the rapid solidification of the melt pool during metal deposition process.

This particular photo represents the temperature variation at $1/5000^{th}$ of a second (shutter speed). Both the response time of the thermocouple and the temperature resolution do not make the thermocouple a suitable candidate for recording temperature in such a short time. Additionally, the thermocouple has been noted as inefficient in acquiring the temperature measurements of the melt pool. An infrared pyrometer provides a non-contact, reliable method for temperature measurement. Infrared pyrometers have been used previously to measure temperature information during 316L SS single track depositions [11] [12].

3. NOMENCLATURE

α = Laser Transmission Efficiency

L_p = Laser Power, (W)

A_S = Area of the Substrate Under the Laser Beam, (m^2)

V_t = Velocity of either the Laser Travel or Table Speed, (m/s)

ρ = Density of the Material, (kg/m^3)

C_s = Specific Heat of the Material in Solid Phase, (J/KgK)

C_l = Specific Heat of the Material in Liquid Phase, (J/KgK)

T = Average Temperature of the Melt Pool, (K)

T_s = Solidus Temperature , (K)

T_l = Liquidus Temperature, (K)

T_m = Melting Temperature, (K)

T_∞ = Ambient Temperature, (K)

H_f = Latent Heat of Fusion, (K)

T_p = Temperature of the Pre - Heated Powder Entering the System , (K)

$\Delta T_p = T_p - T_\infty$, (K)

β_{pwd} = Efficiency of the Powder Flow

$\dot{m_f}$ = Mass Flow Rate, (Kg/sec)

A_e = Area of the Meltpool, (m^2)

ϵ = Emmisivity of the Material

σ = Stefan Boltzman's Contant

k = Effective Conduction Heat Transfer Coefficient, (W/m^2K)

4. MODEL FORMULATION

4.1. BASIC ASSUMPTIONS

To establish a reasonable model for the metal deposition process, some assumptions and key features must be stated which are as follows:

- The metal deposition process was assumed to be in a quasi-stationary state.
- The laser was assumed to move at a constant speed both parallel to the y-axis and perpendicular to the substrate. In reality, the part moves with respect to the laser while the laser beam remains stationary. Thus, the process is stationary in a reference frame attached to the laser beam.
- The radius of the powder particles in the flow was assumed to remain constant.
- The shadowing effect by powder particles was assumed to be negligible. In addition, the laser radiation reflected from either the melt pool or the particles in the powder stream is not considered to add significantly to the input energy. Both of these assumptions were reasonable due to the typically low volumetric fraction of powder.

4.2. ASSUMPTION OF VALUES

- All thermo-physical properties were considered to be independent of the temperature.
- The values of both B and h_{fg} in the overall evaporative model of Choi et al.[13] is material dependant. The value of iron was taken as a good approximation to common ferrous materials[6].

- Room temperature was assumed to be 300 K.
- The powder particles were heated upto 333 K in the powder feeder before the powder particles enters the system. This temperature is dependent on the powder feeder system and can vary from system to system.
- The substrate was measured to reach 500 K during deposition.

4.3. EMPERIMENTAL ASSUMPTIONS

- The melt pool created on the substrate was considered circular in the traverse plane. This slowly changes to ellipse as the laser beam began to move and the solidification front developed.
- The model was valid for conditions where the energy input to the system is equal to the energy required to create a deposit after taking into account the amount of energy lost during the process. Thus a proper balance has to be established between the energy entering the system and the sums of energy required to create a melt pool and to melt the incoming powder.
- The model could be applied to cases where the tracks have a consistent aspect ratio.
- The profile of the laser beam in the experiment should be noted to have a top-hat intensity profile.

4.4. MASS BALANCE

The mass balance equation represents the amount of mass both entering in and sustained by the system under consideration. This system is illustrated diagrammatically in Figure 5.

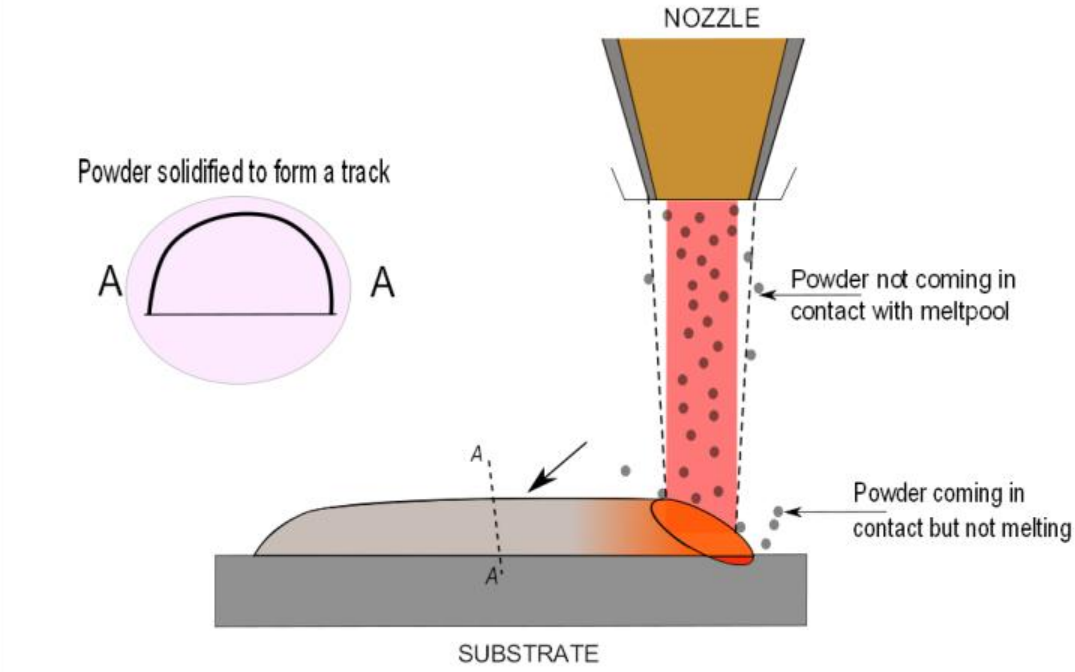

Fig. 5 Representation of the mass both entering in and sustained by the system during deposition.

The mass (of powder particles) flowing in the melt pool can be considered as the amount of mass entering the system which is given by

$$M_{in} = \beta_{pwd}\dot{m}_f \quad (1)$$

where the β_{pwd} is the efficiency of the powder flow and m_f is the mass flow rate (g/sec). Not all powder delivered by the nozzle comes in contact with the melt pool. Thus, a powder flow efficiency was used to compensate this amount denoted by β_{pwd}. Figure 6 is a photograph illustrating a typical powder flow process during deposition.

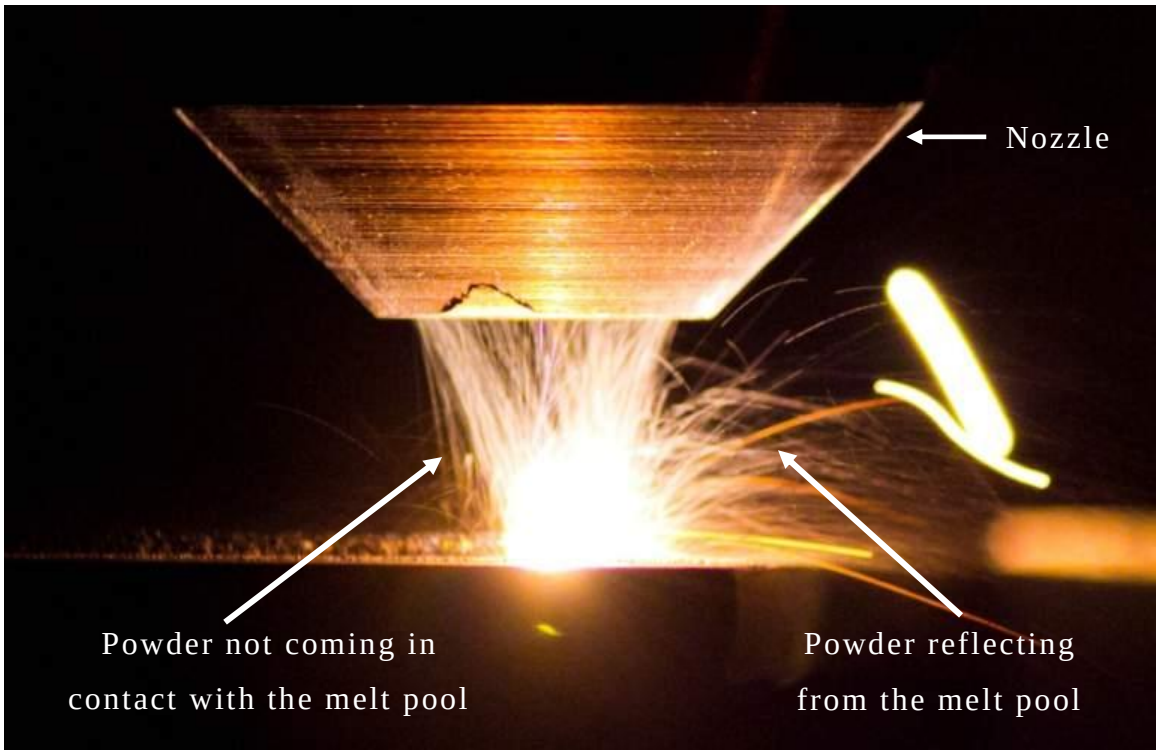

Fig. 6 Photograph of the powder flow process shot during the experiment.

The amount of mass in the system of interest was calculated by

$$M_{sus} = \rho A_{dep} V_t + \beta_{pwd}(1 - \beta_c)\dot{m}_f \quad (2)$$

The first term in Equation 2 represents the amount of mass present in the deposited track. Here, A_{dep} represents the area of the cross-section of the deposited track (m^2), V_t represents the table speed (m/s), and ρ is the density of the powder material (kg/m^3). The cross-sectional area of the deposited track was considered a parabola for calculation purposes. The shape parameters for this parabola are the height of the deposited track (h) and the width of the deposited track (w). Thus, the area of the cross-section of the deposited track can be given by

$$A_{dep} = \frac{2}{3}hw \tag{3}$$

Because the width of the deposited track varies by the energy input per unit length, this research has not assumed it to be equal to the diameter of the laser beam. The second term in Equation 2 represents the amount of powder delivered by the nozzle but which has failed to form a part of the melt pool. This term is effectively represented by β_c, the catchment efficiency, which represents the efficiency with which the powder that enters the melt pool becomes melted to form a part of the deposited track. Thus, the entire mass balance equation can be written as

$$\underbrace{\beta_{pwd}\dot{m}_f}_{\text{Mass added to the system}} = \underbrace{\rho\left(\frac{2}{3}hw\right)V_t}_{\text{Mass in the solidified track}} + \underbrace{\beta_{pwd}(1-\beta_c)\dot{m}_f}_{\text{Mass lost during the process}} \tag{4}$$

The first term on the right side of the Equation 4 gives the total mass present in the deposited track; the second term represents the amount of powder lost during

deposition. The left side of Equation 4 represents the amount of powder flowing into the melt pool through the nozzle. Thus, the deposition height can be obtained by

$$h = \frac{3}{2}\frac{\beta_{pwd}\beta_c \dot{m}_f}{w\rho V_t} \tag{5}$$

In summary, the amount of material being solidified is balanced by both the material added to the melt pool and the material that is lost.

4.5. ENERGY BALANCE

Figure 7 illustrates the system boundary considered for energy balance.

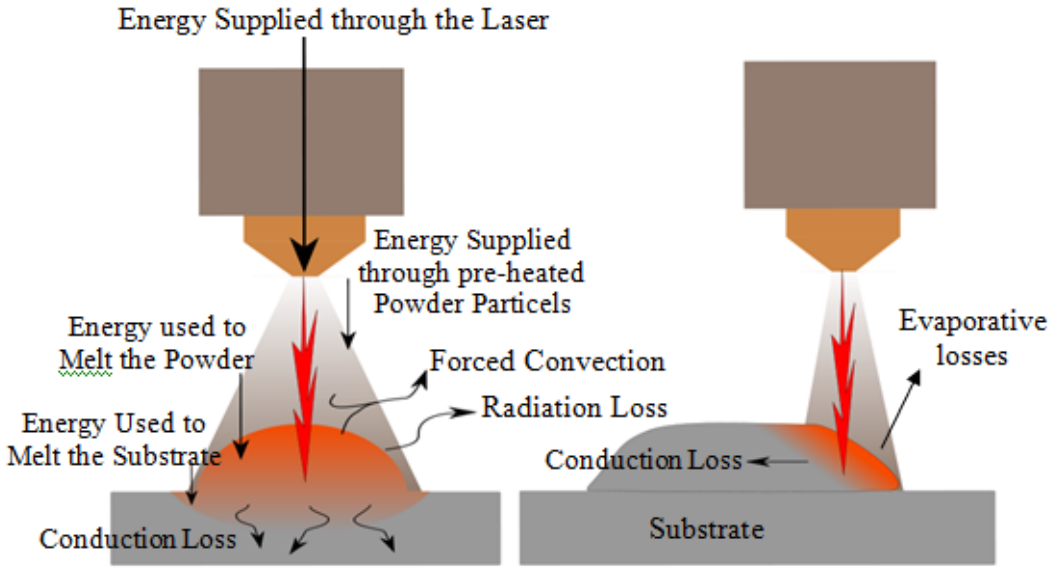

Fig. 7 Energy balance of the deposition process.

The model was constructed in terms of energy flow both into and out of the system, as indicated in Figure 7. The system was assumed to be in a quasi-stationary state. According to Li et al. [14], energy enters the system in one of two methods. In the first method, the laser beam irradiates on the surface of the substrate at a specific energy level. Therefore, the laser energy absorbed by the substrate can be approximated as

$$E_L = \alpha L_p \tag{6}$$

Here, L_p represents the laser power (J/s). α is the laser efficiency which takes into account the laser surface coupling efficiency and the transmission efficiency. Thus α depends on the absorptivity of the material and the conditions of the surface on which deposition is to be made. The value of α is taken as 0.45 for 316L both stainless steel and diode lasers [15], [16].

The second method by which energy enters the system is through the pre-heated powder particles that fall into the melt pool. The powder is pre-heated in the powder feeder before it travels to the nozzle tip. These powder particles have been reported to become heated by the laser beam during their time of flight from the nozzle tip to the melt pool. This consideration leads to a cumbersome calculation. This calculation makes the model suitable for theoretical purposes only rather than for practical applications. Hence, the energy absorbed by the powder particles during their time of flight can be neglected. The total amount of energy entering the system E_{in} can be calculated as

$$E_{in} = \alpha L_P + \beta_{pwd} \dot{m}_f C_s \Delta T_p \tag{7}$$

Here, C_s is the specific heat of the material in a solid state. This value is determined by the material which is to be deposited. The term ΔT_p is the difference of the ambient temperature from temperature of the pre-heated powder particles.

4.5.1. Formation of Melt Pool. As the laser beam strikes the substrate surface, it creates a circular melt pool on the surface of the substrate. In this melt pool, powder particles are injected and, as the laser beam moves, these particles both melt and solidify to form a deposited track. During this process, the circular melt pool gradually builds due to material addition and transforms to an ellipse as shown in the Figure 8.

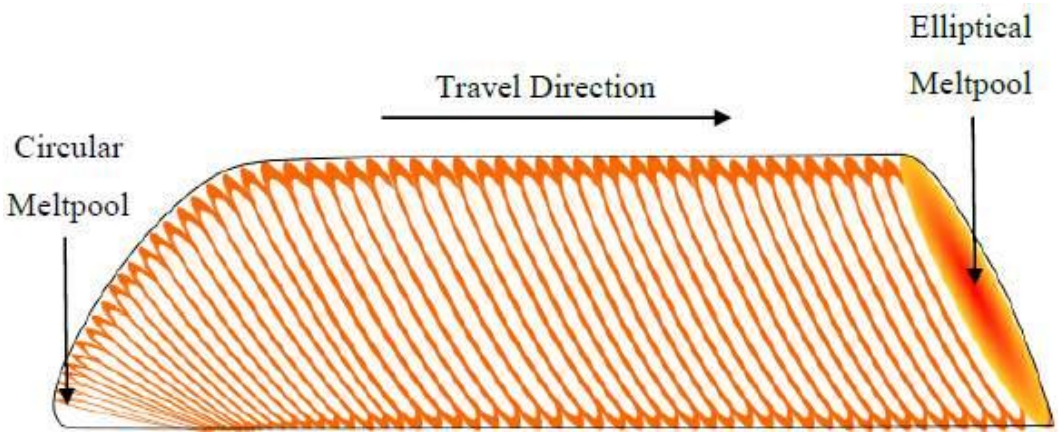

Fig. 8 The transition of the melt pool from circle to ellipse during the deposition process.

Part of the ellipse is on the raised track where the material is both melted and deposited. The other part is formed on the horizontal surface to melt the substrate.

Of the total energy supplied to the substrate through both the laser beam and the powder particles, represented by Equation 7, some amount of the energy is conducted to the substrate and the rest is used to melt the incoming powder particles. Thus the energy utilized to both create the melt pool and melt the incoming powder is approximated by

$$E_m = [A_{dep} * V_t * \rho * \{(C_s(T_s - T_\infty) + H_f + C_l(T_m - T_s)\}] +$$
$$[\beta_{pwd} * \dot{m_f} * (C_s(T_m - T_p) + H_f + C_l(T - T_m))] \quad (8)$$

where A_s area of the beam spot (m^2), V_t is the table speed (m/s^2), ρ is the density of the substrate material (kg/m^3), C_s and C_l are the specific heats of the material in solid and liquid phase (J/KgK). The first part of Equation 8 represents the melting of the substrate to create a melt pool. Thus, the value of the specific heat should be taken for the substrate material. The second part of Equation 8 represents the energy required to both melt the incoming powder particles and create a deposition track. Here, Equation 8 contains the phase interaction term which accounts for the latent heat that is either absorbed or released during melting and solidification according to the amount of mass flowing in the system.

4.5.2. Energy Loss from the System. The laser beam conducts energy to the substrate when it strikes the surface. Some portion of this energy is used to melt both the substrate and powder which is the useful energy as represented by Equation 8. The remaining energy is absorbed by the substrate through lattice vibration and is considered excess energy. Thus, by applying Fourier's law, the energy lost due to conduction can be written as

$$E_{cond} = k * A * (T - Tsubs) + k * Ae * (T - T_l) \quad (9)$$

where k is the effective thermal conductivity of the material ($W/m^{2}K$) which is taken into account by considering the thickness of the substrate and the mean conduction length

through the deposited track, T_{subs} is the substrate temperature during deposition (K). Here, the second term represents the energy conducted to the deposited track by the melt pool. The areas taken in both the first and second term differ according to the description previously given. Energy loss due to convection is negligible when compared with energy loss due to conduction, radiation, and the total energy absorbed by the workpiece [17]**.** The melt pool is always shielded by a constant flow of argon gas. This gas acts as a carrier gas for the powder particles. Thus, the effect of the forced convection on the melt pool can be approximated as

$$E_{conv} = h_c * Ae * (T - T_\infty) \tag{10}$$

Here, the value of h_c, the convective coefficient of the argon gas, is taken from the experimental results of Giacobbe [18]. The temperature of the melt pool (K) is represented by T. The ambient temperature (K) is represented by T_∞. Energy loss through radiation can be approximated by the Stefan-Boltzman's rule, given as

$$E_{rad} = A_e * \varepsilon * \sigma * (T^4 - T_\infty^4) \tag{11}$$

where ε is the emissivity of the melt surface, and σ is the Stefan Boltzmann's constant (W/m^2-K). Both the evaporative and boiling losses have been shown to contribute to the energy loss from the melt pool. But experimental results, however, have concluded that the losses due to evaporation were more significant as compared to the convective losses [19]. For LMD process, the boiling losses can be ignored as they are insignificant as

compared to evaporation losses. Thus, the evaporation loss according to the overall evaporation model of Choi et al. [13] is given as

$$E_{evap} = A_e * h_{fg} * e^{\left\{B+6.1210-\left(\frac{18836}{T}\right)-0.5\log T\right\}} \quad (12)$$

Here, the value of B is dependent on both the material property and the latent heat of vaporization h_{fg}, as stated in [13]. Finally, of the total powder that comes in contact with the melt pool, some are reflected and some are lost. These powder particles, however, absorb partial energy from the melt pool and/or laser beam. Thus, energy lost through powder that comes in contact with the melt pool (but fails to become part of the melt pool) is given as

$$E_p = \beta_{pwd} * (1-\beta_c) * \dot{m}_f * C_p * (T_s - T_p) \quad (13)$$

where β_c is the catchment efficiency, and T_p is the temperature of the pre-heated powder particles(K). Quasi-stationary state conditions must be established for energy to remain balanced. Most thermodynamic models assume a quasi-stationary although the complex travel path of the deposition nozzle gives transient heat flow. This state is established very quickly. Thus,

$$E_{in} = E_m + E_{Cond} + E_{Conv} + E_{Rad} + E_{evap} + E_p \quad (14)$$

where E_{in} is the energy entering the system, E_m is the energy required to melt the material, E_{Cond} is the energy lost due to conduction, E_{Conv} is the energy lost due to

forced convection, E_{Rad} is the energy lost due to radiation, E_{evap} is the energy lost due to evaporation, and E_p is the energy absorbed by the powder particles which have failed to form a part of the deposited track. The model is now complete. Both the verification of the model and application are stated in the following sections.

5. MODEL VERIFICATION AND DISCUSSION

5.1. EXPERIMENTAL PROCEDURE

The proposed model was verified by conducting several experimental runs. Figure 9 displays the experimental set-up used for both deposition and local temperature measurement.

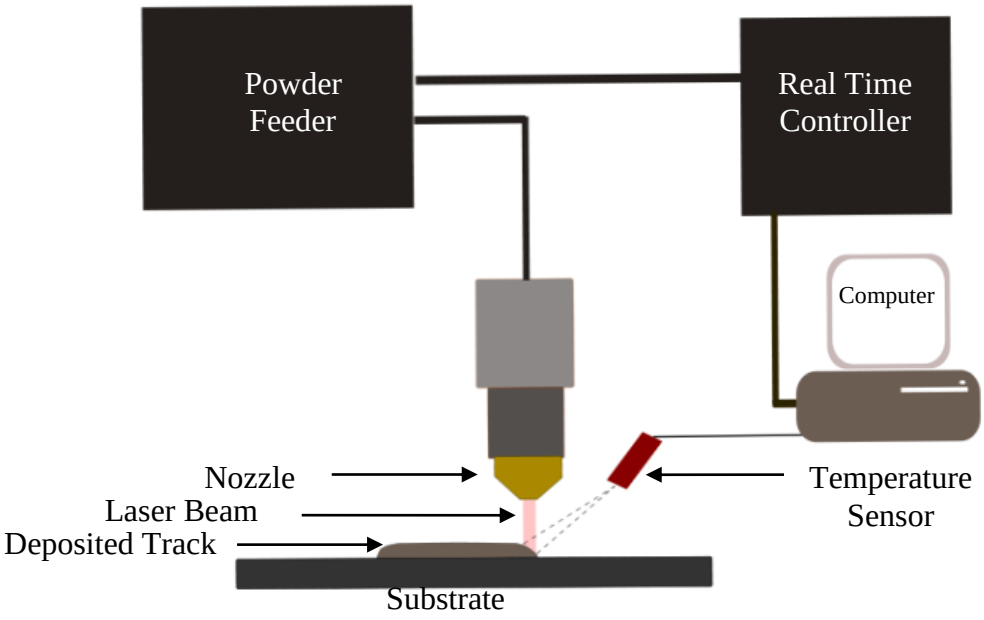

Fig. 9 Diagrammatic representation of the experimental set up.

This experiment was performed with a laser metal deposition system. This system contained of a laser system, a powder feeder unit, a 5-axis CNC machine, and a monitoring system. The laser system used in the experiment was ISl-1000M Laser Diode System manufactured by Nuvonyx Inc. It was able to produce a single wavelength fiber couple diode laser of upto 1kW, operating in continuous wave mode (800nm). Stainless

steel (316L) was used as a deposition material on a mild steel substrate. The thermo-physical properties of both materials tested are listed in Table 1.

Table 1 Thermo-physical properties of the materials used during the experiment.[6, 20]

Property	316L Stainless Steel	Mild Steel
Solid Specific Heat (J/Kg K)	490	481
Liquid Specific Heat (J/Kg K)	510	502
Thermal Conductivity (W/m K)	21.5	22
Density (kg/m^3)	8000	7200
Latent Heat of Fusion (J/Kg)	2.5×10^5	2.47×10^5
Solidus Temperature (K)	1600	1750
Liquidus Temperature (K)	1710	1800
Latent Heat of Vaporization (J/Kg)	6.2595×10^6	7.34×10^6
Ambient Temperature (K)	300	
Stefan-Boltzman's constant	5.67×10^{-8}	

The value of the laser surface efficiency, the catchment efficiency, and the powder flow efficiency were selected at 0.45, 0.9, and 0.85 respectively, for calculation purposes [6, 21]. These values were highly dependent on the system. Single path deposition tracks were conducted to validate the model. The size of the substrates used measureds 0.5 inch wide, 0.25 inch thick, and 2 inch in length. The experimental

parameters are given in Table 2. The stand-off distance between the coaxial nozzle and the deposition surface was kept at 8 mm to keep the focal plane coinciding with the deposition surface at all times. The melt pool temperature was measured with a dual-wavelength non-contact temperature sensor (MI-GA 5-LO). This sensor was capable of effectively decreasing disturbance from both powder and dusts. The response time of the sensor was 2 ms. Thus, the sensor returned a graph of the melt pool temperature, with respect to time through a computer. From this, the maximum temperature was considered at the melt pool temperature for every particular set of process parameters.

After the deposition, all samples were initially sectioned to obtain a flat cross section. These cross sectioned samples were then cold mounted in a mounting resin. This was followed by etching with a 2% Nital to reveal the grain boundaries. After etching, all samples were examined with a Hi-Rox Optical Microscope to capture the images. ImageJ software was used to measure the required bead dimensions after proper calibration. The bead dimensions were measured as shown in the Figure 10. Gauge R&R was also performed to assess the variation associated with the measurement system. The precision-to-total ratio was calculated to be 0.001163. This calculation can be considered adequate as it is less than .10. Additionally, the Capability Ratio (CR) of the measurement system was measured to be 0.000962. (A measurement system is considered to be adequate if the CR value is less than .10).

Table 2 Process parameters used for the experiment.

Process Parameters	Values
Laser Power	500, 750, 1000 W
Table Speed	125, 225, 325 mm/min
Powder Flow Rate	16, 24, 32 g/min

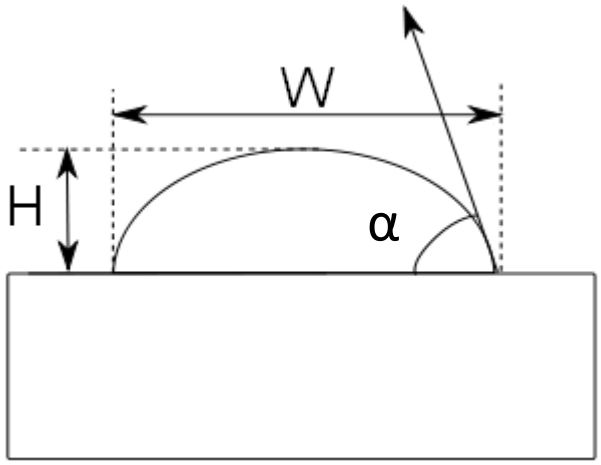

Fig. 10 Measurement of bead geometry.

5.2. MELT POOL TEMPERATURE PREDICTION

Both experimental and model results of the melt pool temperature during the laser deposition process are presented in Figure 11. The results show both the temperature measured by the IR pyrometer during each run and the temperature predicted by the model. The model is successful in predicting the melt pool temperature with an error of $\pm$20%. This error can be attributed to both the number of assumptions as well as the

inconsistency of the process. A small (>20%) amount of error being can be considered a good trade-off when compared to the simplicity of the model.

The temperature range fell between 1800-2500K. This range is within the same range predicted by previous models [6] [22]. The model, primarily, over predicts the actual temperature. The estimation however, is good. The modeled results are also consistent within the entire range of the experimental values.

Thus, the modeled temperature can be used during the process design stage by the manufacturing engineer. Hence, model is in good agreement with the experimental work.

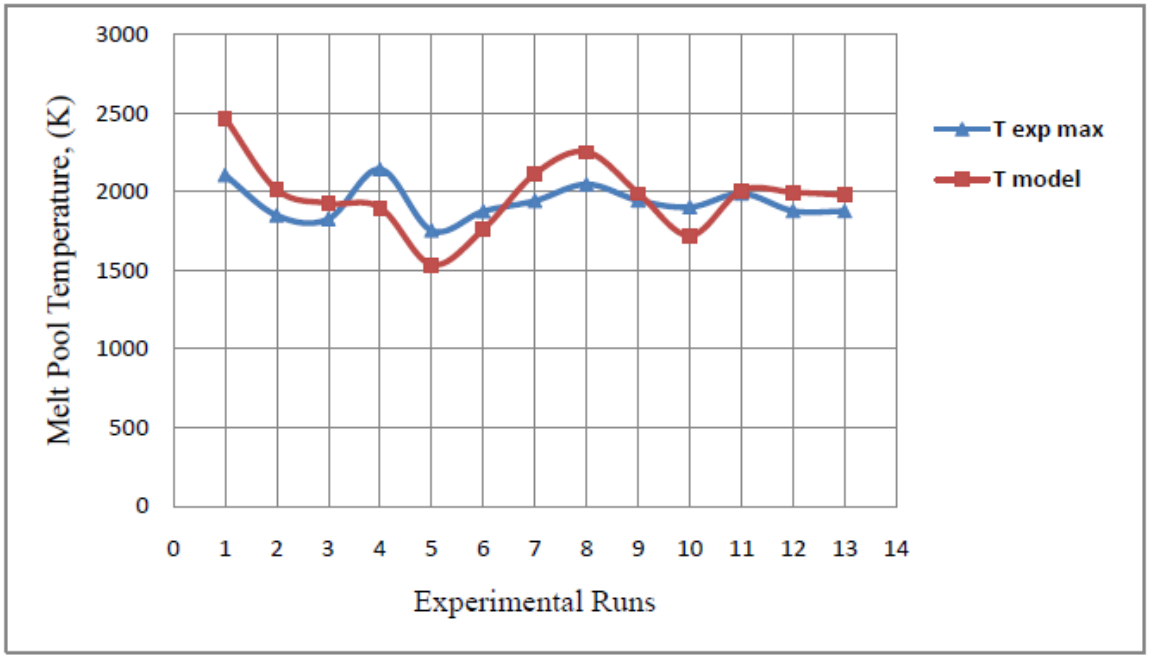

Fig. 11 Comparison of the modeled and the experimental results of the temperature in the melt pool.

Table 3 displays the results of ANOVA performed between the experimentally measured and modeled temperature. No statistical difference exists between the

experimentally measured and modeled temperature because the P-value is greater than 0.74 [23].

Table 3 Results of ANOVA performed between the experimentally measured and modeled melt pool temperatures.

ANOVA						
Source of Variation	SS	df	MS	F	P-value	F_{crit}
Between Groups	3990.62	1	3990.62	0.105	0.74	4.25
Within Groups	911903.44	24	37995.97			
Total	915894.07	25				

5.3. HEIGHT PREDICTION

Both the temperature of the melt pool and the height of the track are the two most important parameters during the manufacturing of the part geometry by the metal deposition process. Figure 12 illustrates the macroscopic images of the cross sections of the weld beads.

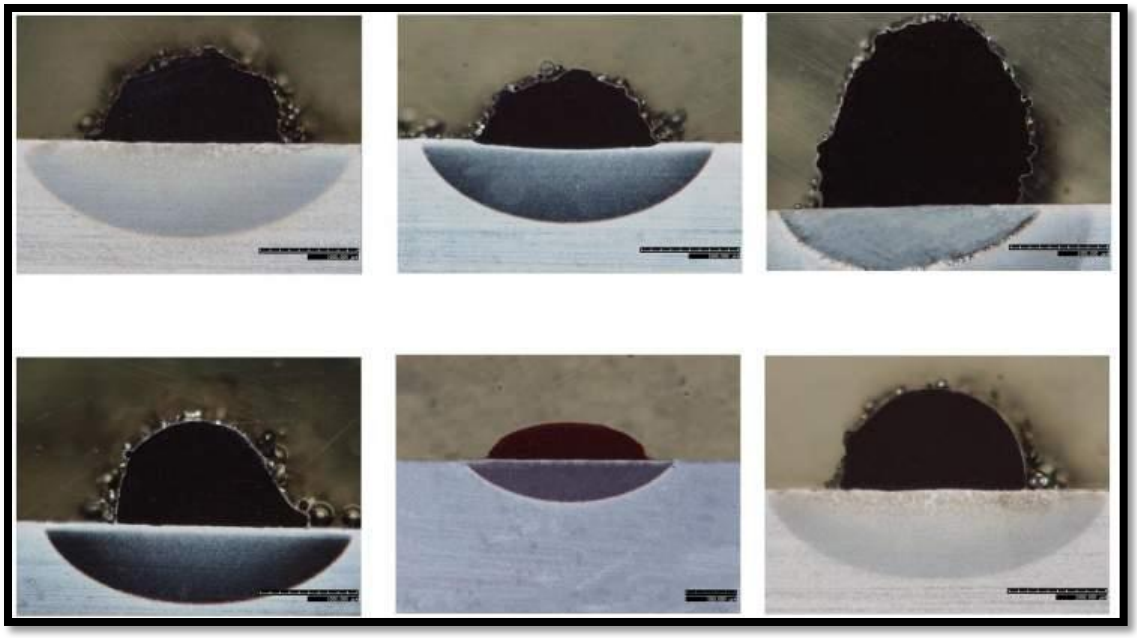

Fig. 12 Macrographs of the bead geometries deposited during the experiments.

Figure 13 presents the comparison between the measured and the predicted value of the height. Some degree of error appears between the predicted and the measured value.

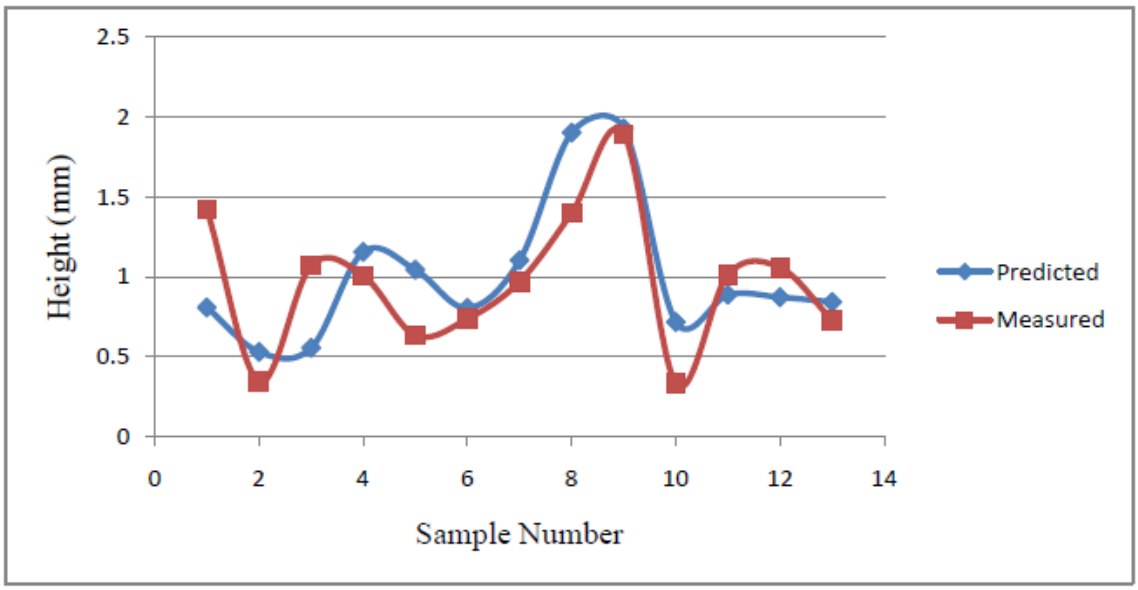

Fig. 13 Comparison of the predicted and measured heights of the deposited tracks without the error function.

The amount of useful energy (given by the amount of laser power) supplied to the substrate affects the catchment efficiency. A simple correction factor can be introduced comparing both the measured and the predicted heights with the amount of useful energy supplied during the process as shown in Equation 15. Figure 14 shows the comparison of the modeled and measured height after introducing the error function.

$$h = \frac{3}{2}\frac{\beta_{pwd}\beta_c \dot{m}_f}{w\rho V_t \emptyset} \tag{15}$$

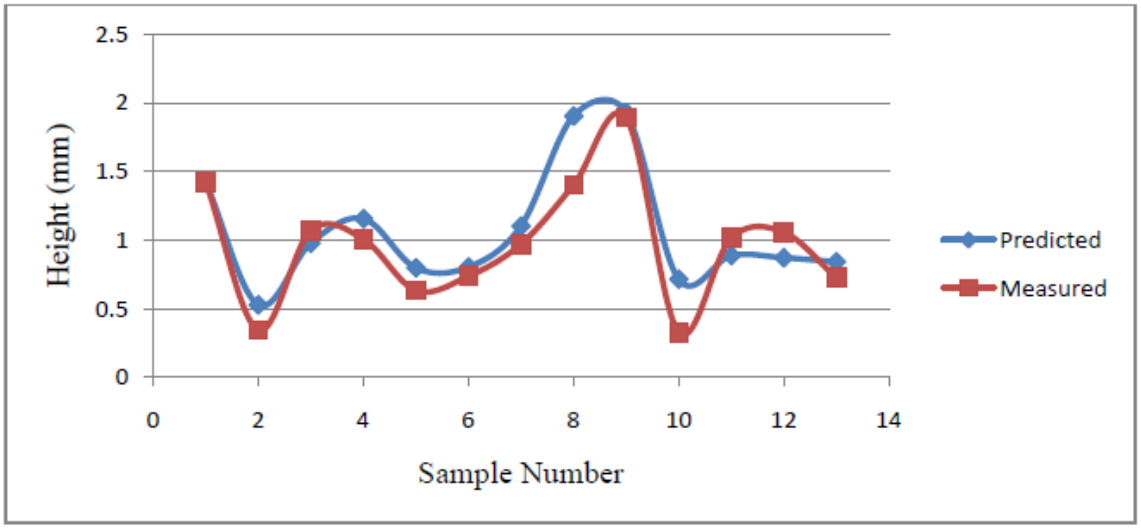

Fig. 14 Comparison of the modeled and the measured height after the use of error function.

Table 4 gives the results of ANOVA performed between the experimentally measured and the modeled height after using the correction factor. No statistical difference exists between the modeled and the experimentally measured heights as the P-value is greater than 0.05 [23]. If the rate of energy per unit area was less than 200

J/sec/mm^2, then the value of was 0.105. This indicates that, as the useful energy decreases, the efficiency of the system is also reduced.

Table 4 Results of ANOVA performed between the experimentally measured and modeled weld bead height.

ANOVA						
Source of Variation	SS	df	MS	F	P-value	F crit
Between Groups	0.067	1	0.067	0.359	0.554	4.259
Within Groups	4.539	24	0.189			
Total	4.607	25				

The weaker melt pool does not have sufficient energy to sustain all of the powder fed to it. Similarly, if the rate of energy per unit area is more than 200 J/sec/mm^2, then the value of ϕ is 0.6. This also indicates a variation in the catchment efficiency with respect to the useful energy supplied to the substrate. The term ϕ depends on the type of laser beam source, the laser intensity profile, the energy supplied to the substrate, and the diameter of the laser beam.

5.4. THE WELD BEAD ANGLE, ASPECT RATIO AND THE SUPERHEAT

Figure 15 displays the trend in both the weld bead angle and the aspect ratio (W/H) over the range of superheat measured in the weld bead. The weld bead angle

increases with the amount of superheat but becomes stable after approximately 300K of superheat.

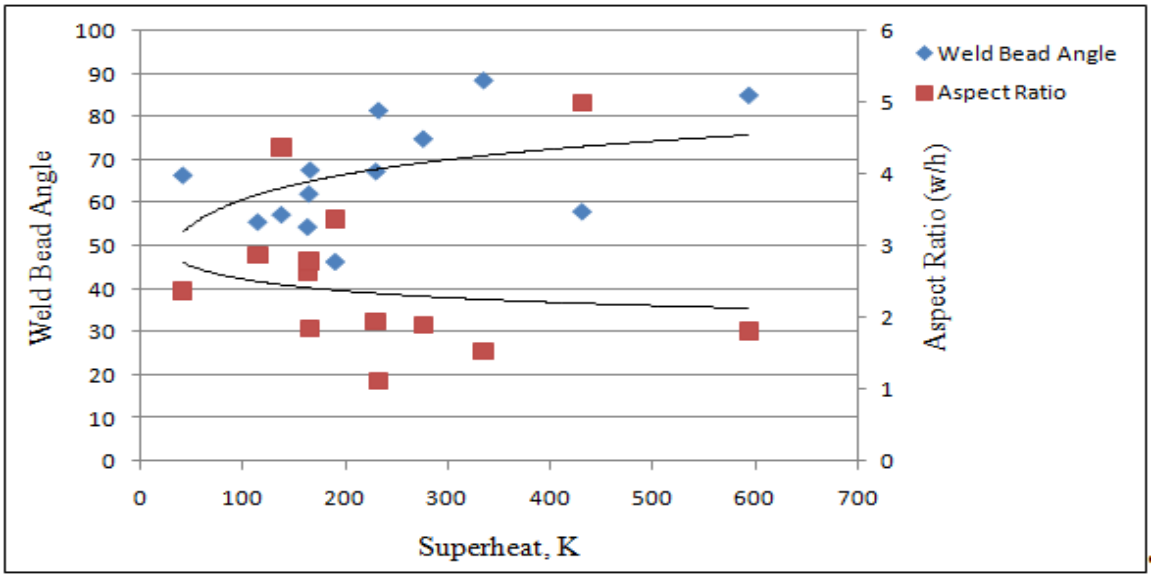

Fig. 15 Comparison of the amount of superheat with the weld bead angle and the aspect ratio of the beads.

The additional superheat may increase the weld bead angle. The chances of failed deposit, however, also increase significantly. This failed deposit means the metal tends to flow more than what is required to create a bead shape resulting in a non-conforming surface. Thus, the optimum level of superheat to be given in the bead for a specific bead angle must be decided. This is due to the fact that the surface tension gradient varies with the temperature in the melt pool [24]. If a change in the temperature coefficient of the surface tension is positive, $\frac{\partial \sigma}{\partial T} > 0$, then the direction of the fluid flow, shown in Figure 16 (b) results in 'B' and 'C' type of bead profiles. Similarly, a low superheat results in a

negative temperature coefficient of surface tension, $\frac{\partial \sigma}{\partial T} < 0$, which results in 'A' type profiles shown in Figure 16 (a).

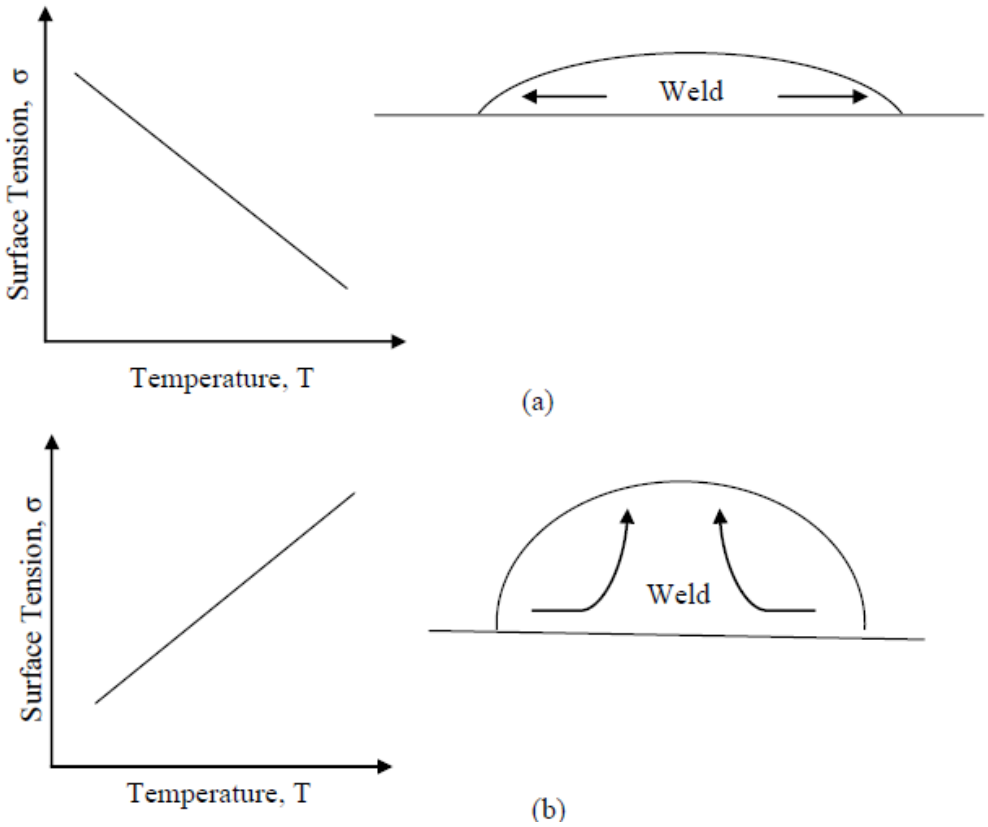

Fig. 16 Effect of the positive and negative value of $\boldsymbol{\partial \sigma / \partial T}$ in the weld bead.

Thus, optimizing the temperature coefficient of surface tension would lead to producing bead with the desired profiles. Figure 15 displays the variation of the aspect ratio with the amount of superheat. The bead becomes both wider and flatter as the aspect ratio becomes higher, which shapes the bead as 'A' type profiles. Similarly, an aspect ratio nearer to 1 represents a narrow, taller bead profile. This profile can be represented

by both ‘B’ and ‘C’ type profiles. A positive value of the temperature coefficient of surface tension can be represented by beads whose aspect ratios are low and weld bead angles are high. Similarly, an aspect ratio close to the weld bead angle on the graph represents a negative value of temperature coefficient of surface tension.

5.5. VARIATION IN THE WIDTH OF THE WELD BEAD

Figure 17 displays the variation of the width of the weld bead with the amount of useful energy. The amount of useful energy is calculated by subtracting the energy lost due to various losses from the total energy supplied to the melt pool. The width of the weld bead varies considerably and is not equal to the radius of the laser beam (2.5 mm in the experimental set-up). Thus, considerable power attenuation exists, justifying, the assumption that the radius of the melt pool is not equal to the radius of the laser beam. Ideally, the diameter of the laser beam should be equal to the width of the weld bead.

This can be attributed to the interaction time of the laser beam interacting with the substrate surface where the melt pool is formed. The interaction time is the duration during which laser energy is focused on the substrate to create a melt pool. Interaction time depends on both the table speed and the length of the deposit. A longer interaction time means more energy is supplied to the substrate when both the laser power and the mass flow rate are constant.

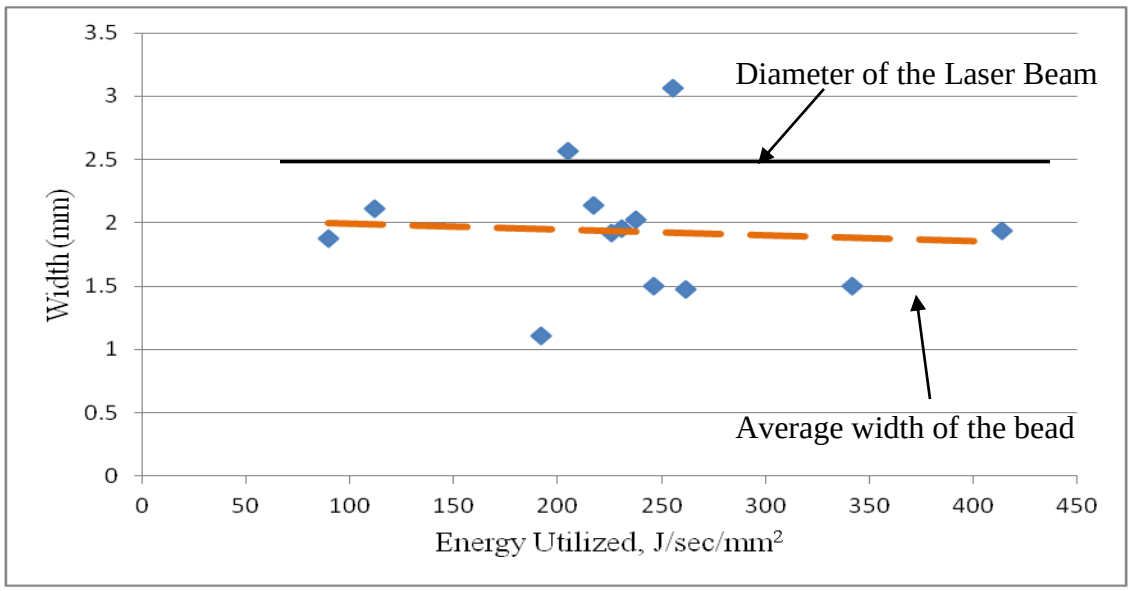

Fig. 17 Comparison of the width of the weld bead with the energy utilized during the process.

Figure 18 illustrates the variation in the width of the bead, at different table speeds, with both a constant laser power and a constant mass flow rate. At the same laser power and mass flow rate, the width of the bead is inversely proportional to the table speed. At lower table speeds, the interaction time is more. Hence, more energy is transferred to the substrate. Additionally, at the same laser power and table speeds, the increase in mass flow rate increases the bead width.

This means that the melt pool still has the capacity to form a bead with a higher aspect ratio. The low variation in the bead width at both 1000W laser power and 32 g/min mass flow rate indicates that, at both levels of table speed, the melt pool had sufficient energy to melt the incoming powder. This variation in width can be attributed to the blocking effect.

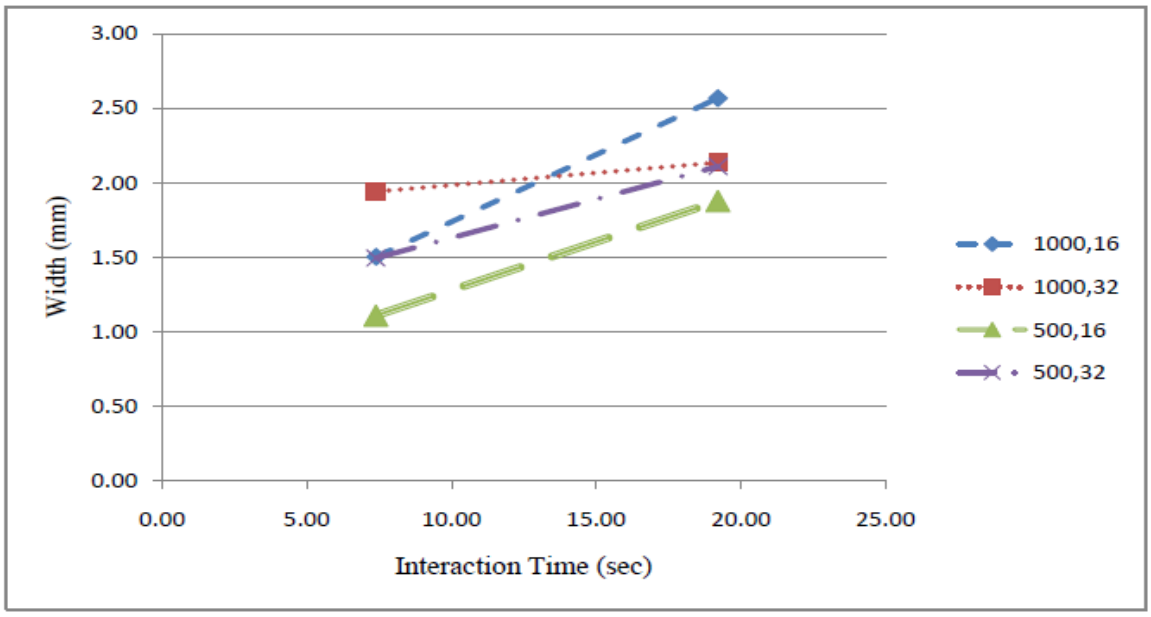

Fig. 18 Variation of the bead with interaction time for different laser power and mass flow rates.

As explained previously, during the deposition process, as the laser moves with a specified table speed, the melt pool transforms from a circle to an ellipse. As the laser moves ahead and the deposition process begins, this ellipse acts like a moving melt pool. (Note that, in the Figure 8, part of this ellipse is on the substrate) During a long interaction time, the ellipse moves ahead slowly thus allowing the substrate to melt. This melted substrate forms a bead with a width equal to that of the diameter of the laser beam. Thus the melt pool blocks the heat from flowing to the substrate. In summary, both the interaction time and the blocking effects play an important role in determining the width of the weld bead.

5.6. ENERGY DISTRIBUTION

Figure 19 presents energy distribution during the laser deposition process, obtained from the proposed model. The individual energy pathways have been averaged

for all runs in consideration; they are used here to represent the pathways diagrammatically.

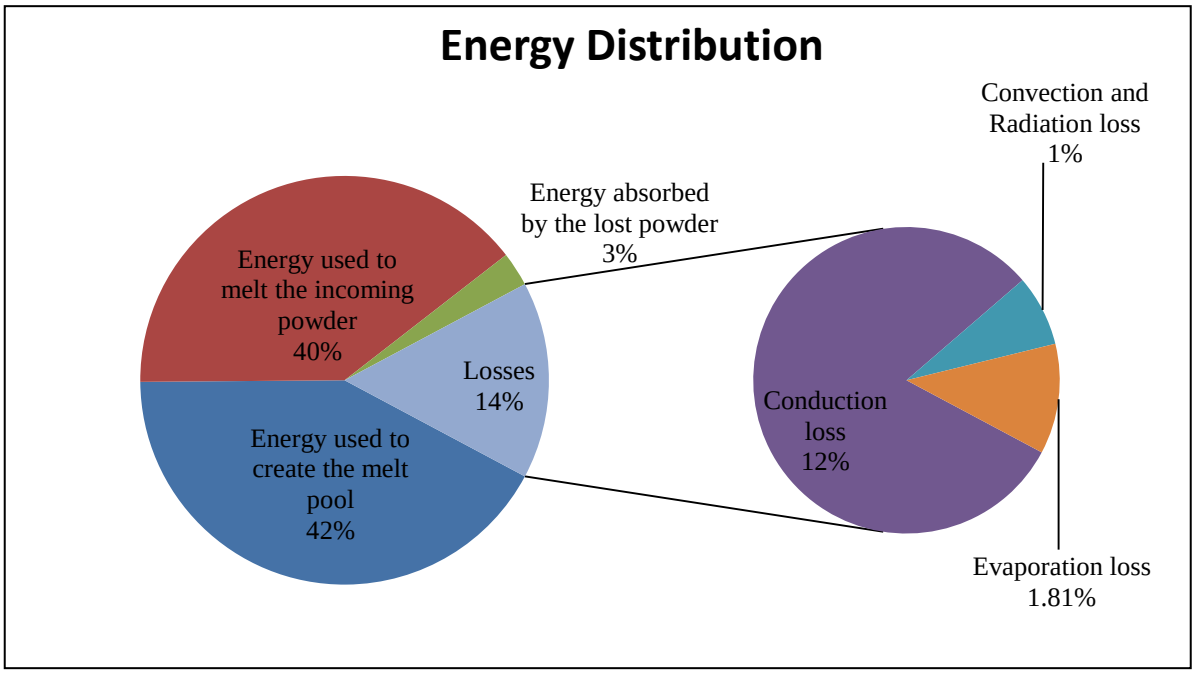

Fig. 19 Average distribution of modeled energy lost from the system.

The efficiency with which the laser power is supplied to the melt pool is just 45% for a diode laser. More than half of the energy input to the system is lost. Of the total energy that reaches the substrate, conduction losses account for the majority from the melt pool at all power levels. Thus, much energy is conducted to the substrate, becoming a part of the non-useful energy.

Not all energy conducted to the substrate can be termed as a part of the energy lost due to conduction. Some amount of the same energy is required to both create a melt pool and make the fusion possible. Both radiation and evaporation losses come next in

terms of energy lost, accounting for nearly 6% of the total losses. The energy lost due to forced convection can be considered as negligible and is in agreement with the experimental results of Vasinota et al. [25]. Thus, both natural and forced convection losses can be ignored as they are negligible when compared to losses due to both conduction and radiation. The results of the modeled energy distribution due to various losses are in agreement with the results of Pinkerton and Li [6].

6. MODEL APPLICATION

The section is aimed at shedding some light on the proper application this model. This section provides a method for applying this model generated in section 4. A relationship between the weld bead angle and the superheat is generated, which can be used in conjunction with this model.

A realistic input to the model can be considered a 'weld bead angle.' Figure 15 has, therefore, been plotted again by switching the ordinate abscissa in Figure 20 to calculate the required superheat.

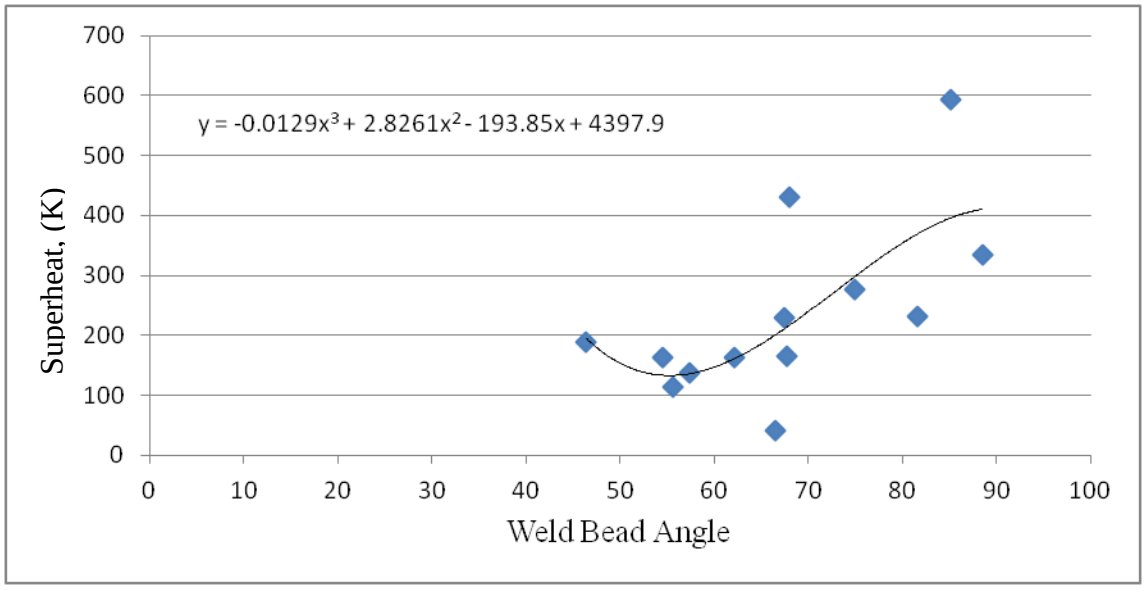

Fig. 20 Variation of the weld bead angle with the amount of superheat.

An approximation to the data can be cubic, which is given by the equation in the graph. Thus, both a proper bead angle was selected and the amount of superheat required was calculated from Figure 20. The expected temperature across the melt pool was

estimated according to the amount of superheat needed. This temperature was used as the input value to the energy balance Equation 14. Two cases arise as follows:

Case 1: User specifies the bead height: In such a case, because the system of equations does not have any physical constraints, both the mass flow rate and the table speed may be negative. Therefore, iterations should be performed on the specified height to obtain realistic results.

Case 2: Specifying the bead height from the co-relationship in Figure 15: In such a case, a better approximation of bead height can be achieved using the curve fit data. Hence, the number of iterations to obtain realistic results will be reduced. In case the user needs a height other than one obtained from Figure 15, this value can be considered as a good initial point. Additionally, further iterations can be performed.

Thus, a linear set of two non-linear equations with three unknowns (laser power, table speed, and mass flow rate) are obtained. At this stage, the mass flow rate is fixed. This is done to ensure the energy input to the system is sufficient to create a melt pool. A number of iterations must be performed to obtain a suitable value for both the mass flow rates and the table speed. Figure 21 is a flowchart of the step-by-step application for the proposed planning tool.

Depositions were carried out based on these values. The macrographs of the beads are given in Figure 22. These values do not indicate any type of defect, such as either porosity or lack of fusion. Table 5 displays the geometrical results of the beads produced on the basis

of the proposed model. Both the expected and the measured values of the bead geometry are in good agreement.

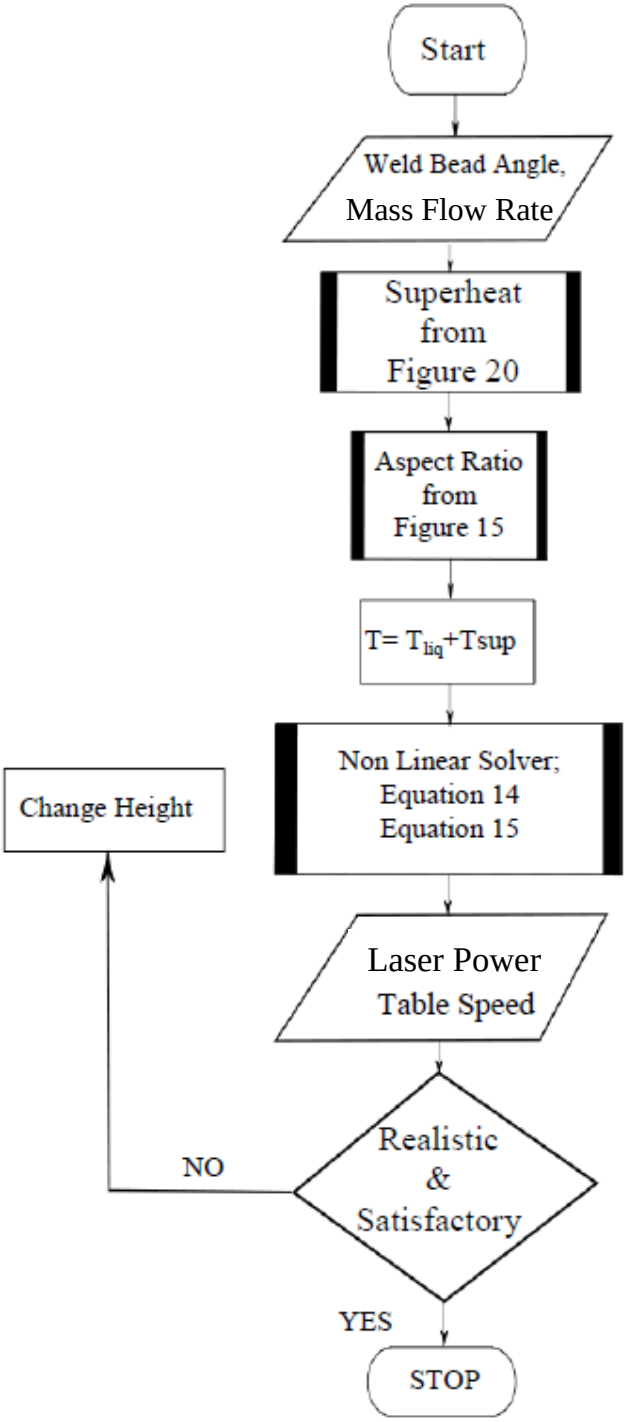

Fig. 21 Schematic diagram of the flowchart of the proposed model.

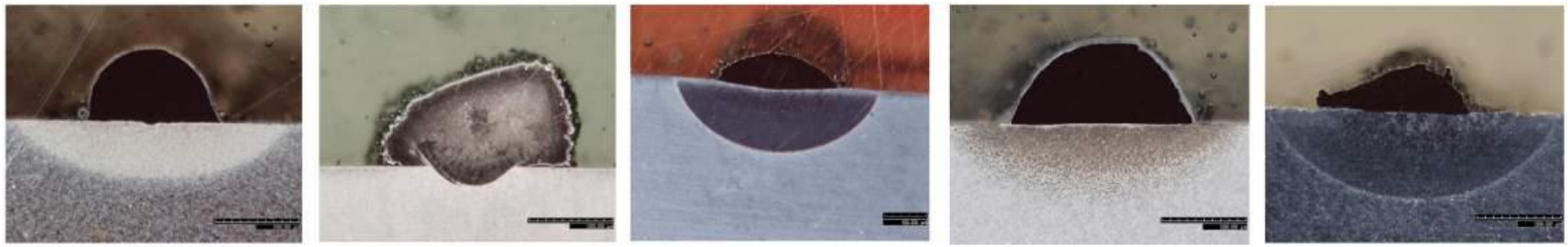

(a) (b) (c) (d) (e)

Fig. 22 Macrographs of the deposited track with a pre-determined bead angle at 100X magnification.

Table 5 Properties for the track deposited using the model.

Property	(a)		(b)		(c)		(d)		(e)	
Weld Bead Angle	Expected	Measured	Expected	Measured	Expected	Measured	Expected	Measured	Expected	Measured
	60	72	75	92	30	39	45	57	35	47
Aspect Ratio	2.01		2.45		2.09		2.35		2.16	
Superheat (K)	325		400		722		221		522	
Laser Power (W)	1000		750		750		500		500	
Mass Flow Rate (g/min)	30		16		18		16		12	
Table Speed (mm/min)	225		85		250		225		245	

7. CONCLUSION

A model was created to predict the temperature of the melt pool during the laser deposition process. This model is based on the energy flow, both in and out, of the melt pool. The model considers the effect of the material heating, powder heating, wastage of powder, and various losses during the process. Temperature averaging across the melt pool was predicted effectively by establishing both the mass and the energy balance at the melt pool boundaries. The height of the deposited tracks has also been predicted effectively using the proposed constants.

This model was experimentally verified and the results are in good agreement with the prediction. A novel idea of using the superheat present in the melt pool was both proposed and applied in this research. The amount of superheat present in the melt pool was found to be directly proportional to the weld bead angle. Increasing the amount of superheat can also result in non-conforming bead shapes. Thus, a narrow band of useful superheat exists within which the operation must be carried out. Additionally, the model has been applied to produce beads of both the desired weld bead angle and the aspect ratio using different substrate materials and sizes. In the future, this design tool can be developed for multi-layered deposition to examine the validity of this idea for multi-layered tracks.

8. ACKNOWLEDGEMENT

This research is a result of the phenomenal support and guidance extended to me by various individuals at Missouri University of Science & Technology. I would like to express my sincere thanks to my advisor, Dr. Frank Liou, who has been a constant source of encouragement and guidance for me.

Secondly, I would like to thank both Mr. Todd Sparks and Dr. Jianzhong Ruan for their advice at each step during my research. Finally, I would like to thank both the National Science Foundation and Intelligent Systems Center for supporting this research financially.

9. REFERENCES

1. Steen, W.M., Weeresinghe, V.M.; Monson, P.: *Some aspects of the formation of laser clad tracks.* SPIE, 1986. **650**: p. 226-234.

2. Colaco, R.; Costa, L.; Guerra, R.; and Vilar, R.: *A simple correlation between the geometry of laser cladding tracks and process parameters* in *Proc. 1994 NATO Advanced Study Institute Conf. on Laser Processing: Surface Treatment and Film Deposition,*1994.

3. Kar, A.; and Mazumder, J.: *One-dimensional finite-medium diffusion model for extended solid solution in laser cladding of Hf on nickel.* Acta Metallurgica, 1988. **36**(3): p. 701-712.

4. Jouvard, J.M.; Grevey, D.F.; Lemoine, F.; and Vannes, A.B.: *Continuous wave Nd : YAG laser cladding modelling: a physical study of track creation during low power processing.* J. Laser Appl., 1997. **9**(1): p. 43.

5. Gedda, H.; Powell, J.; Wahlstrom, G.; Li, W.B.; Engstrom, H.; and Magnusson, C.: *Energy redistribution during CO 2 laser cladding.* J. Laser Appl., 2002. **14**(2): p. 78.

6. Pinkerton, A.J.; and Li, L.: *An analytical model of energy distribution in laser direct metal deposition.* Proceedings of the Institution of Mechanical Engineers, Part B: Journal of Engineering Manufacture, 2004. **218**(4): p. 363-374.

7. Toyserkani, E.; Khajepour, A.; and Corbin, S.: *3-D finite element modeling of laser cladding by powder injection: effects of laser pulse shaping on the process.* Optics and Lasers in Engineering, 2004. **41**(6): p. 849-867.

8. Yi Liu, C.;Lin, J.: *Thermal processes of a powder particle in coaxial laser cladding.* Opt. Laser Technol., 2003. **35**(2): p. 81.

9. Griffith, M.L.; Schlieriger, M.E.; Harwell, L.D.; Oliver, M.S.; Baldwin, M.D.; Ensz, M.T.; Essien, M.; Brooks, J.; Robino, C.V.; Smugeresky, J.E.; Hofmeister, W.H.; Wert, M.J.; Nelson, D.V.: *Understanding thermal behavior in the LENS process.* Materials and Design, 1999. **20**(2-3): p. 107-113.

10. Griffith, M.L.;Ensz, M.T.; Puskar, J. D.; Robino, C.V.; Brooks, J. A.; Philliber, J. A.; Smugeresky, J. E.; Hofmeister, W. H.: *Understanding the microstructure and properties of components fabricated by Laser Engineered Net Shaping (LENS).* 2000.

11. Ahsan, M.N.; and Pinkerton, A.J.: *An analytical-numerical model of laser direct metal deposition track and microstructure formation.* Modelling and Simulation in Materials Science and Engineering, 2011. **19**(5).

12. Doubenskaia, M., Bertrand, Ph.; and Smurov, I.: *Pyrometry in laser surface treatment.* Surface and Coatings Technology, 2006. **201**(5): p. 1955-1961.

13. Salcudean, M., Choi, M.; and Greif, R.: *A study of heat transfer during arc welding.* International Journal of Heat and Mass Transfer, 1986. **29**(2): p. 215-225.

14. Li, W.B.; Engstrom, H.; Powell, J.; Tan, Z.; and Magnusson, C.: *A simple correlation between the geometry of laser cladding tracks and process parameters.* in *Proc. 5th Conf. on Laser Material Processing in the Nordic Countries,* 1995.

15. Liou, F.; Choi J.; Landers, R.; Janardhan, V.; Balakrishnan, S.N.; and Agarwal, S.; *Research and development of a hybrid rapid manufacturing process*. in *Proceedings 12th Annual Solid Freeform Fabrication Symposium*. 2001. Austin, Texas.

16. Boddu, M.; Musti, S.; Landers, R.; Agarwal, S.; and Liou, F.:. *Empirical modeling and vision based control for the laser metal deposition process*. in *Proceeding 12th Annual Solid Freeform Fabrication Symposium*. 2001. Austin, Texas.

17. Kumar, S.; and Roy, S.: *Development of theoretical process maps to study the role of powder preheating in laser cladding.* Computational Materials Science, 2006. **37**(4): p. 425-433.

18. Giacobbe, F.W.: *Determination of gaseous heat transfer coefficients at elevated temperatures.* Applied Thermal Engineering, 2005. **25**(2–3): p. 205-225.

19. Landram, C.S.:*Measurement of Fusion Boundary Energy Transport During Arc Welding.* Journal of Heat Transfer, 1983. **105**(3): p. 550-554.

20. *ASME Metals Handbook*, 1990, ASM International, Metals Park, Ohio.

21. Han, L.; Phatak, K..; and Liou, F.: *Modeling of laser cladding with powder injection.* Metallurgical and Materials Transactions B, 2004. **35**(6): p. 1139-1150.

22. Hofmeister, W.; Wert, M.; Smugeresky, J.; Philliber, J.A.; Griffith, M.; and Ensz, M.; *Investigating Solidification with the Laser-Engineered Net Shaping (LENS^{TM}) Process.* Journal of Metals, 1999. **51**(7).

23. Montgomery, D.C.: *Design and Analysis of Experiments*. 5th ed 2001, New York: John wiley & Sons Incs. .

24. Li, Z.; Mukai, K.; Zeze, M.; Mills, K.: *Determination of the surface tension of liquid stainless steel*, in *Journal of Materials Science*2005, Springer Netherlands. p. 2191-2195.

25. Vasinonta, A.; Beuth, J.L.;and Griffith, M.: *Process Maps for Predicting Residual Stress and Melt Pool Size in the Laser-Based Fabrication of Thin-Walled Structures.* Journal of Manufacturing Science and Engineering, 2007. **129**(1): p. 101-109.

VITA

Sriram Prabhu, son of Tejovati Prabhu and Sirish Prabhu, was born in Baroda, India. He received his B.E. in Mechanical Engineering from Maharaja SayajiRao University of Baroda, Gujarat, India in July 2010. In August 2010, he joined Missouri University of Science and Technology to pursue his Masters in Manufacturing Engineering. Sriram worked as a Graduate Research Assistant in the Laser Aided Manufacturing Processes Lab at Missouri S&T. His research was focused on metal deposition of overhanging features. Sriram earned his Masters in Manufacturing Engineering in July 2012.

Sriram has published a conference paper in the proceedings of the Intelligent Systems Center Symposium at Rolla, Missouri in April 2011. Sriram now intends to join Mailam India Limited, Pondicherry, India as a Research Engineer.